



Radio Science

RESEARCH ARTICLE

10.1029/2018RS006653

Special Section:

URSI General Assembly and
Scientific Symposium (2017)

Key Points:

- GPS signals L2C and L5 are more susceptible to be impacted by ionospheric irregularities
- The statistics of fading scintillation events verified how degraded are the new signals at L2C and L5 in comparison to the L1 signal
- Experimental data show that more severe fading are expected to L2C and L5 signals

Correspondence to:

A. de O. Moraes,
aom@ita.br

Citation:

de O. Moraes, A., Vani, B. C., Costa, E., Sousasantos, J., Abdu, M. A., Rodrigues, F., et al. (2018). Ionospheric scintillation fading coefficients for the GPS L1, L2, and L5 frequencies. *Radio Science*, 53, 1165–1174. <https://doi.org/10.1029/2018RS006653>







Received 31 MAY 2018

Accepted 23 AUG 2018

Accepted article online 7 SEP 2018

Published online 28 SEP 2018

Ionospheric Scintillation Fading Coefficients for the GPS L1, L2, and L5 Frequencies

Alison de O. Moraes¹ , Bruno C. Vani^{2,3} , Emanuel Costa⁴ , Jonas Sousasantos⁵ , Mangalathayil A. Abdu⁶ , Fabiano Rodrigues⁷ , Yuri C. Gladek⁸, César B. A. de Oliveira⁵, and João F. Galera Monico³

¹Instituto de Aeronáutica e Espaço/Instituto Tecnológico de Aeronáutica, São José dos Campos, Brazil, ²Departamento de informática, Instituto Federal de Educação, Ciência e Tecnologia de São Paulo—Campus Presidente Epitácio (IFSP-PEP), Presidente Epitácio, Brazil, ³Departamento de cartografia, Universidade Estadual Paulista Júlio de Mesquita Filho, Presidente Prudente, Brazil, ⁴Centro de Estudos em Telecomunicações, Pontifícia Universidade Católica do Rio de Janeiro, Rio de Janeiro, Brazil, ⁵Instituto Tecnológico de Aeronáutica, São José dos Campos, Brazil, ⁶Instituto Tecnológico de Aeronáutica/Instituto Nacional de Pesquisas Espaciais, São José dos Campos, Brazil, ⁷William B. Hanson Center for Space Sciences, University of Texas at Dallas, Richardson, TX, USA, ⁸EMBRAER, São José dos Campos, Brazil

Abstract The terrestrial ionosphere over low-latitude regions presents the unique phenomena of the equatorial ionization anomaly (characterized by global maximum in plasma concentration) and plasma-depleted regions known as equatorial plasma bubbles and associated smaller-scale plasma irregularities. Transionospheric radio signals such as those from Global Navigation Satellite Systems constellations, traveling across this ambient, may suffer severe scintillation in amplitude and phase due to these plasma structures. Presently, three civilian signals available for GPS users, at L1 (1575.42 MHz), L2C (1227.60 MHz), and L5 (1176.45 MHz) are used to investigate the propagation effects due to these irregularities. The purpose of the present work is to evaluate statistically the distribution of severe fade events for each of these carrier frequencies based on the nonlinear ionospheric propagation effects as represented by the fading coefficients of α - μ distribution. The results from the analyses of data sets recorded by stations at different geomagnetic latitude locations in Brazil show that regions closer to the equatorial ionization anomaly crest present higher probability of severe fade events. Additionally, the L5 signals, dedicated for safety-of-life applications, revealed more unfavorable results when compared to the L1 and L2C frequencies. The results further showed that for $0.8 \leq S_4 \leq 1.0$ the probabilities of fades deeper than -10 dB were between 8.0% and 6.5% depending on the station position. Considering the case of fades deeper than -20 dB, the results reach values near 1%, which is quite concerning. These results show empirically the fading environment that users of the new civilian signals may experience in low-latitude region. Additionally, the fading coefficients may help in the comprehension of the distribution of amplitude scintillation and its relation with the frequency used, aiding in the future the development of signal processing algorithms capable to mitigate errors for navigation users.

Plain Language Summary This work shows differences in the statistics of GPS signals at different frequencies. The results warn that new signals will be more affected by the ionosphere in regions of low latitudes.

1. Introduction

In the equatorial and low-latitude regions, a conjunction of several electrodynamics mechanisms may give rise to large-scale plasma depletions in the *F* region of the ionosphere, which are usually referred to as equatorial plasma bubbles (EPBs). These structures, generated in the equatorial ionosphere, map along the magnetic flux tubes to higher latitudes with larger background plasma density, a region known as the equatorial ionization anomaly (EIA), with crests generally located within the geomagnetic latitude intervals ($+12^\circ$, $+20^\circ$) and (-12° , -20°). After reaching the mature state, the plasma bubbles usually drift eastward. Plasma bubble structures present longitudinal extensions reaching a few hundreds of kilometers. Inside the main structure, secondary instabilities occur, producing smaller-scale irregularities. This random medium produces amplitude and phase scintillation of radio signals that propagate through the ionosphere, causing positioning errors, losses of phase lock, and consequently performance degradation and

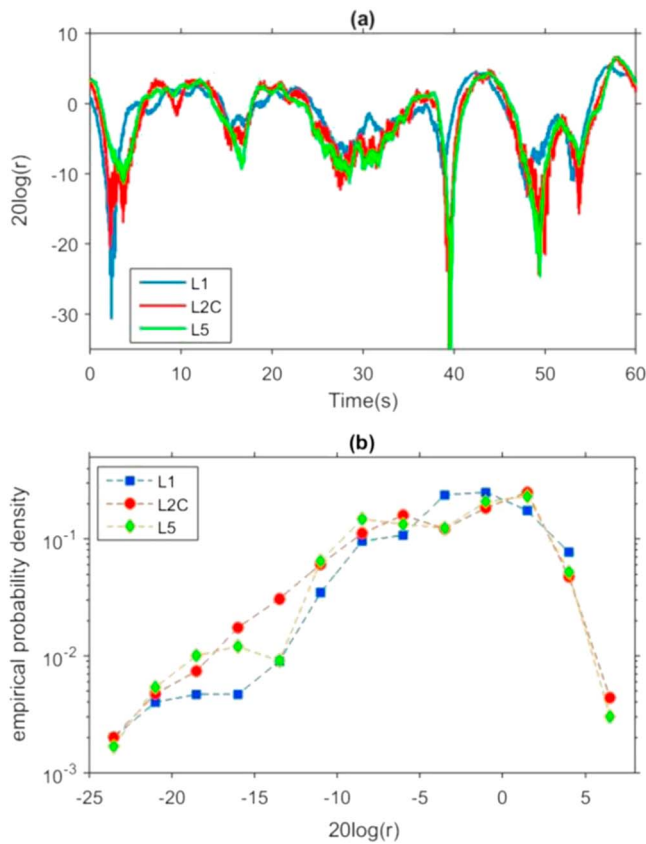


Figure 1. (a) GPS scintillation recorded at Presidente Prudente on 9 November 2014 for the L1, L2C, and L5 signals of PRN 25; (b) corresponding empirical probability density function of $[20 \log(r)]$ for the three signals, where r^2 represents values of the normalized received power.

to establish how scintillating signals may create availability issues to users of the GPS L2C and L5 frequencies.

Figure 1a illustrates one example of scintillation on 1-min records of the GPS L1, L2C, and L5 signals of PRN 25, measured by the Presidente Prudente monitor on 9 November 2014. The greater severity of the scintillation phenomenon in the L2C and L5 signals are observed at several time instants. Figure 1b shows the corresponding empirical probability density function (pdf) of $[20 \log(r)]$ for the three signals, where r^2 represents values of the normalized received power. Each r^2 value is computed from the measured in-phase In and quadrature Qd components of the received signal through $r^2 = (In^2 + Qd^2) / \langle (In^2 + Qd^2) \rangle$, where $\langle \rangle$ represents the ensemble average over 1 min of data. This plot highlights the severity of the fade events for the new signals L2C and L5, in particular for the range between -10 and -20 dB. Considering the example of Figure 1, it is possible to find the pair of α - μ coefficients that better represents the empirical distribution of the received power for each frequency. These fading coefficients, in association with the selected distribution, characterize scintillation at each frequency.

The period of analysis, observation locations, geophysical conditions, and associated data sets will be described in the following section. The α - μ distribution will be briefly revisited in section 3, presenting the most important equations and highlighting the benefits of this model for statistical characterization of fading events. In section 4, the results from a statistical analysis performed for the L1, L2C, and L5 frequencies will be presented and discussed, providing an idea on how much more affected the users of new signals will be. Finally, the section 5 will summarize the main results of this study and present concluding remarks.

unavailability of service in receivers of the Global Positioning System (GPS). Under severe scintillation scenarios, GPS receiver tracking loops may experience deep power fades accompanied by abrupt phase shift transitions causing receiver loss of lock (Humphreys et al., 2009). Furthermore, Seo et al. (2011) highlighted that when GPS receivers experience deep fades no performance standards are specified for aviation users, which is a concern.

More recently, Jiao et al. (2016) showed that fading events are specially pronounced on L2C (1227.60 MHz) and L5 (1176.45 MHz) signals and that the amount of fades deeper than 15 dB may reach 10 times the number of similar events on L1 (1575.42 MHz) signals, depending on location. In Moraes, Muella, et al. (2017), a statistical analysis compares the occurrence of scintillation in the Global Navigation Satellite System L1 and L2 frequency bands. The results show that during the summer and spring seasons, the probability of intense scintillation events in the southern crest of the anomaly (dip -12° to -20°) is approximately twice that observed around the geomagnetic equator. Another aspect of the scintillation analysis worth mentioning is the statistical characterization of fading distribution: Moraes et al. (2012) have shown that the GPS radio scintillating signals are better characterized by the α - μ model (Yacoub, 2007). This model has one more degree of freedom than a previous and frequently used one (the Nakagami- m distribution). The additional degree is used to model the deep-fade region of the distribution with added flexibility and precision (Moraes, de Paula, et al., 2014). Following Conker et al. (2003), Moraes, Costa, et al. (2014) proposed an extended model based on the α - μ distribution to explain how receivers with the same level of scintillation experience different values of error.

Motivated by these previous studies, this work aims at statistically analyzing the severity of fades due to ionospheric irregularities in the new GPS signals in comparison with those in the traditional L1 signal, with basis on the α - μ fading coefficients. The main objective of the present study is to characterize the deep-fade regime of the distributions and

Table 1
Details About the Stations Used in This Work

| Station | Latitude (°) | Longitude (°) | Dip latitude (°) | Available data |
|---------------------|--------------|---------------|------------------|----------------|
| Fortaleza | −3.74 | −38.57 | −8.86 | 139 nights |
| Presidente Prudente | −22.12 | −51.40 | −16.01 | 133 nights |
| São José dos Campos | −23.20 | −45.85 | −19.28 | 140 nights |
| Porto Alegre | −30.07 | −51.11 | −22.32 | 128 nights |

2. Measurements

The data analyzed in this work were acquired at four different stations distributed over the Brazilian territory. Table 1 shows the name, location, and number of nights contributing with data. To position these stations with respect to the EIA, where the most intense scintillation events are observed, it should be remembered that its southern crest is generally located within the geomagnetic latitude interval (−15°, −20°). Thus, we point out that Fortaleza (FZ) is the station closest to the geomagnetic equator where EPBs are generated. Presidente Prudente (PP) and São José dos Campos (SJ), on the other hand, are located near the southern crest of EIA. Finally, Porto Alegre (PA) is in poleward side of the EIA crest, away from the geomagnetic equator.

The positions of the four stations FZ, SJ, PP, and PA can be seen in Figure 2, which additionally shows a vertical total electron content (vTEC) map over the Brazilian region at 02h00 UT on 13 November 2014. The parameter vTEC is theoretically obtained by the integration of the ionospheric electron density along the vertical direction and expressed in TEC units (1 TECu = 10¹⁶ electrons per square meters). The vTEC map is obtained from GPS network; for more detail, see Hernández-Pajares et al. (2009). The depleted regions (indicated by dashed red lines) denote the presence of EPB structures in the EIA, indicated by enhanced TEC values.

The experimental data recorded from the stations listed in Table 1 were measured by Septentrio PolaRxS scintillation monitors with ultralow noise oven-controlled crystal oscillators for GPS L1 (1575.42 MHz), L2C (1227.60 MHz), and L5 (1176.45 MHz) signals at the sampling frequency of 50 Hz. These receivers belong to the CIGALA/CALIBRA network (Vani et al., 2016). The data used in this study were recorded every night from 19h00 LT to 01h00 LT between 1 November 2014 and 30 March 2015. This period corresponds to the maximum of the current solar cycle. Along the period of analysis the mean monthly solar flux values were respectively 155.2, 158.7, 141.7, 128.8, and 126.0 sfu, where 1 sfu = 10^{−22} W·m^{−2}·Hz^{−1} at the wavelength of 10.7 cm. This is the same period analyzed by Moraes, Costa, et al. (2017), being associated with the equatorial spread F season in the Brazilian sector, according to Abdu et al. (1992).

The Septentrio PolaRxS monitor provides a flag indicating the occurrences of cycle slips in the receiver tracking loop, followed by periods of losses of phase lock, as recently discussed in detail by Moraes et al. (2018). In Figures 3, 4, and 6 of that reference, in association with the corresponding discussion, the authors address the aspects of detected cycle slips in terms of the parameters S_4 and α . For brevity, the periods of losses of phase lock will not be further used or discussed in the present analysis.

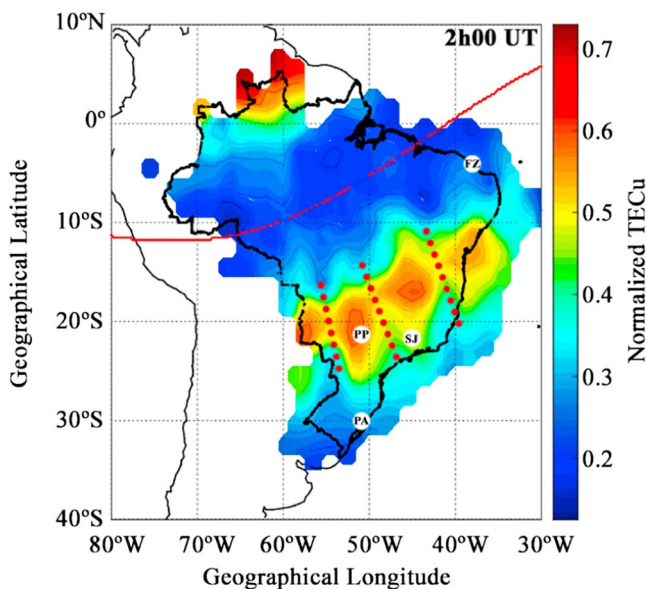


Figure 2. TEC map over the Brazilian region during an equatorial plasma bubble event at 02h00 UT on 13 November 2014. The red dashed lines indicate equatorial plasma bubble structures at low-latitude regions. The position of the four stations FZ, SJ, PP, and PA can also be seen. FZ = Fortaleza; SJ = São José dos Campos; PA = Porto Alegre; PP = Presidente Prudente; TEC = total electron content.

3. The α - μ Distribution

The α - μ model assumes that the received signal results from a composition of clusters of multipath waves that propagated through a nonhomogeneous medium. This model also assumes that the signal is composed of random phases of scattered waves with similar delays within any cluster. For a normalized envelope such that $E[R^2] = 1$, where $I = |R|^2$ is the received signal intensity and R is the amplitude envelope, the α - μ probability density function is given by (Moraes et al., 2012)

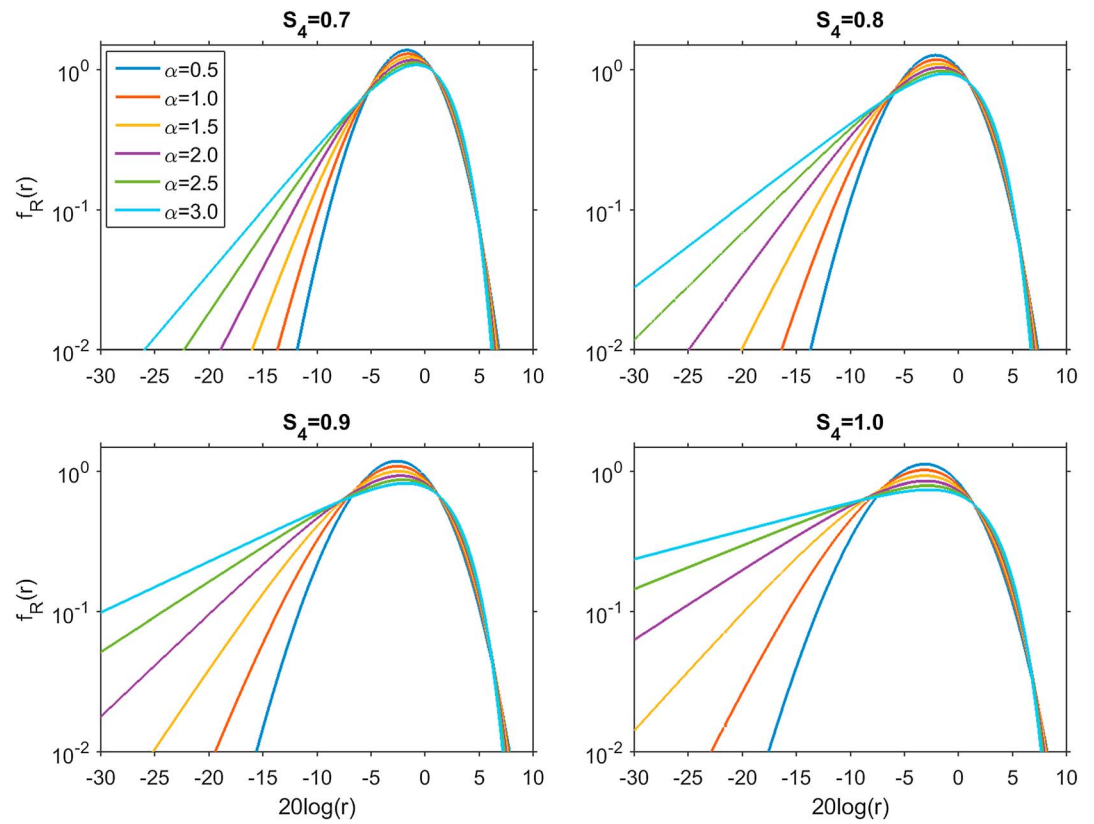


Figure 3. Various shapes of the α - μ probability density function for different fixed values of S_4 , showing the influence of α in the severity of scintillation.

$$f_R(r) = \frac{\alpha r^{\alpha\mu-1}}{\zeta^{\alpha\mu/2} \Gamma(\mu)} \exp\left(-\frac{r^\alpha}{\zeta^{\alpha/2}}\right). \quad (1)$$

In the above expression, $\Gamma(\beta)$ is the Gamma function of general argument β and $\zeta = \Gamma(\mu)/\Gamma(\mu + 2/\alpha)$. According to Yacoub (2007), the α parameter represents the nonlinear function of the modulus of the sum of contributions from the clusters of multipath components from the resulting envelope and the μ parameter represents the real extension of the number of multipath components in the propagation environment, to be estimated by field data.

The severity of amplitude scintillation is commonly represented by the scintillation index S_4 , defined by (Yeh & Liu, 1982):

$$S_4 = \sqrt{\langle I^2 \rangle - \langle I \rangle^2} / \langle I \rangle \quad (2)$$

where $\langle \rangle$ denotes the ensemble average. In practice, temporal averages (1 min) are used.

The relation between the α - μ parameters and the scintillation index S_4 is given by Moraes et al. (2012):

$$S_4^2 = \frac{\Gamma(\mu)\Gamma(\mu + 4/\alpha) - \Gamma^2(\mu + 2/\alpha)}{\Gamma^2(\mu + 2/\alpha)}. \quad (3)$$

Table 2
The μ Values Associated With Each Curve in Figure 3

| | $\alpha = 0.5$ | $\alpha = 1.0$ | $\alpha = 1.5$ | $\alpha = 2.0$ | $\alpha = 2.5$ | $\alpha = 3.0$ |
|-------------|----------------|----------------|----------------|----------------|----------------|----------------|
| $S_4 = 0.7$ | 36.68 | 8.58 | 3.67 | 2.04 | 1.31 | 0.94 |
| $S_4 = 0.8$ | 28.92 | 6.65 | 2.81 | 1.56 | 1.01 | 0.72 |
| $S_4 = 0.9$ | 23.56 | 5.32 | 2.23 | 1.23 | 0.80 | 0.57 |
| $S_4 = 1.0$ | 19.69 | 4.37 | 1.81 | 1.00 | 0.65 | 0.46 |

Equation (3) indicates that there are infinite pairs of α - μ coefficients for a given value of S_4 . The following analyses will concentrate on the values of S_4 , assuming α as a complementary parameter, while μ will be treated as an auxiliary parameter, dependent on the other two (α and S_4) through equation (3). Treating μ as the complementary parameter and α as the

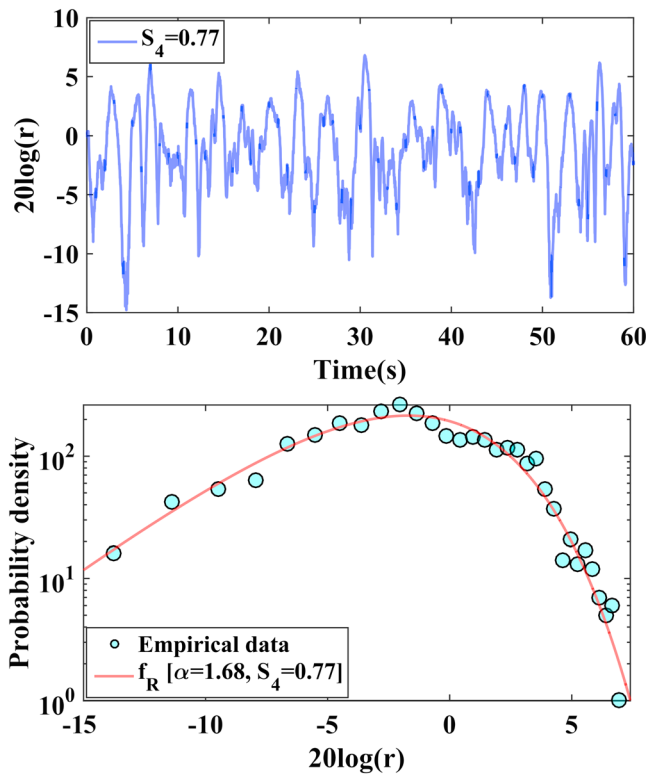


Figure 4. Upper panel: Example of 1-min batch of scintillation data with $S_4 = 0.77$. Lower panel: Associated empirical and theoretical α - μ probability density functions. The latter was estimated with basis on equation (1) and the maximum-likelihood procedure.

auxiliary parameter would also be viable, in principle. However, past studies by Fremouw et al. (1978) and Banerjee et al. (1992) suggested that the Nakagami- m model provided a good fit to empirical distributions. Thus, focusing on α is more intuitive, since the Nakagami- m distribution is a particular case of the α - χ^2 distribution (with $\alpha = 2$). Additionally, it maintains continuity with previous work by Moraes, de Paula, et al. (2014) and Moraes, Costa, et al. (2014), allowing comparisons among empirical distributions, the α - χ^2 model (using S_4 and α), and the Nakagami- m model (using only S_4). Each panel of Figure 3 displays different shapes of $f_R(r)$ for fixed values of S_4 and variable α . It is important to note that, for any fixed value of S_4 , the probability of deep fades increases as α increases. The μ values associated with each curve in Figure 3 are shown in Table 2.

Figure 3 indicates that a signal represented by $f_R(r)$ with $S_4 = 0.7$ and $\alpha = 3.0$ (light blue curve in the upper left panel) will be more threatening to the user than a signal with $S_4 = 0.9$ and $\alpha = 0.5$ (dark blue curve in the lower left panel). The question now is how to estimate the pair of α - μ coefficients that best represents the received signal. In this work, α - μ fading coefficients were estimated by fitting equation (1) to the empirical pdf resulting from each 1-min batch of the available data set with basis on the maximum-likelihood procedure (Venables & Ripley, 2002). Additionally, the α - μ estimates were associated to the corresponding value of S_4 , determined by the direct application of equation (2) to the same data batch. The upper panel of Figure 4 illustrates one example of data batch where $S_4 = 0.77$. The lower batch of Figure 4 shows the associated empirical

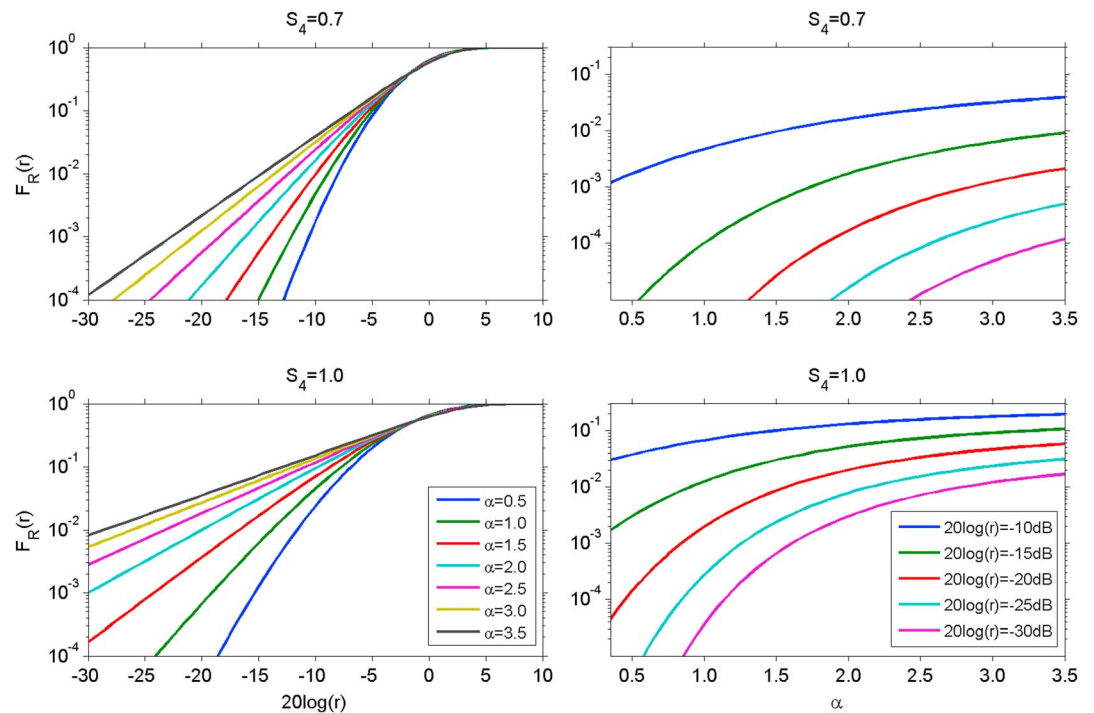


Figure 5. Left panels: Curves for $F_R(r)$ as a function of the signal intensity, assuming two fixed values of S_4 (0.7 and 1.0) and different α values. Right panels: Curves for $F_R(r)$ as a function of α , assuming two fixed values of S_4 (0.7 and 1.0) and different values of the signal intensity.

Table 3
Probabilities of S_4 Occurrences in Different Intervals ($S_4 - 0.05, S_4 + 0.05$) and Locations for the L1, L2C, and L5 Signals

| S_4 | 0.3 | 0.4 | 0.5 | 0.6 | 0.7 | 0.8 | 0.9 | 1.0 | 1.1 | $P_{S_4 \geq 0.3}$ | $P_{S_4 \geq 0.5}$ |
|----------------------------|-------|------|------|------|------|------|------|------|------|--------------------|--------------------|
| Fortaleza | | | | | | | | | | | |
| P_{L1} (%) | 6.27 | 2.50 | 1.19 | 0.49 | 0.31 | 0.12 | 0.05 | 0.04 | 0.01 | 10.98 | 2.21 |
| P_{L2C} (%) | 11.22 | 5.37 | 2.60 | 1.46 | 0.92 | 0.57 | 0.24 | 0.14 | 0.07 | 22.59 | 6.00 |
| P_{L5} (%) | 11.13 | 5.49 | 2.74 | 1.63 | 1.05 | 0.60 | 0.35 | 0.14 | 0.09 | 23.22 | 6.60 |
| Presidente Prudente | | | | | | | | | | | |
| P_{L1} (%) | 4.98 | 4.17 | 3.26 | 2.90 | 2.15 | 1.71 | 1.01 | 0.66 | 0.30 | 21.14 | 11.99 |
| P_{L2C} (%) | 3.98 | 3.45 | 3.25 | 3.19 | 3.05 | 2.90 | 2.35 | 1.60 | 0.91 | 24.68 | 17.25 |
| P_{L5} (%) | 3.59 | 3.36 | 3.05 | 2.99 | 3.06 | 3.13 | 2.63 | 1.79 | 1.04 | 24.64 | 17.69 |
| São José dos Campos | | | | | | | | | | | |
| P_{L1} (%) | 3.24 | 2.33 | 1.86 | 1.35 | 1.26 | 1.09 | 0.98 | 0.81 | 0.47 | 13.39 | 7.82 |
| P_{L2C} (%) | 3.12 | 2.44 | 2.00 | 1.78 | 1.69 | 1.60 | 1.63 | 1.38 | 0.82 | 16.46 | 10.90 |
| P_{L5} (%) | 2.99 | 2.29 | 1.97 | 1.80 | 1.69 | 1.79 | 1.73 | 1.51 | 0.86 | 16.63 | 11.35 |
| Porto Alegre | | | | | | | | | | | |
| P_{L1} (%) | 0.83 | 0.53 | 0.41 | 0.34 | 0.28 | 0.24 | 0.27 | 0.22 | 0.14 | 3.26 | 1.90 |
| P_{L2C} (%) | 0.88 | 0.54 | 0.49 | 0.43 | 0.35 | 0.42 | 0.42 | 0.38 | 0.22 | 4.13 | 2.71 |
| P_{L5} (%) | 0.83 | 0.53 | 0.50 | 0.42 | 0.32 | 0.42 | 0.46 | 0.43 | 0.23 | 4.14 | 2.78 |

and estimated pdfs of the received intensity. The latter is based on equation (2) using the estimated coefficients $\alpha = 1.68$ and $\mu = 2.35$.

The cumulative distribution function $F_R(r)$ for the α - μ model when $E[R^2] = 1$ can be directly determined from equation (2):

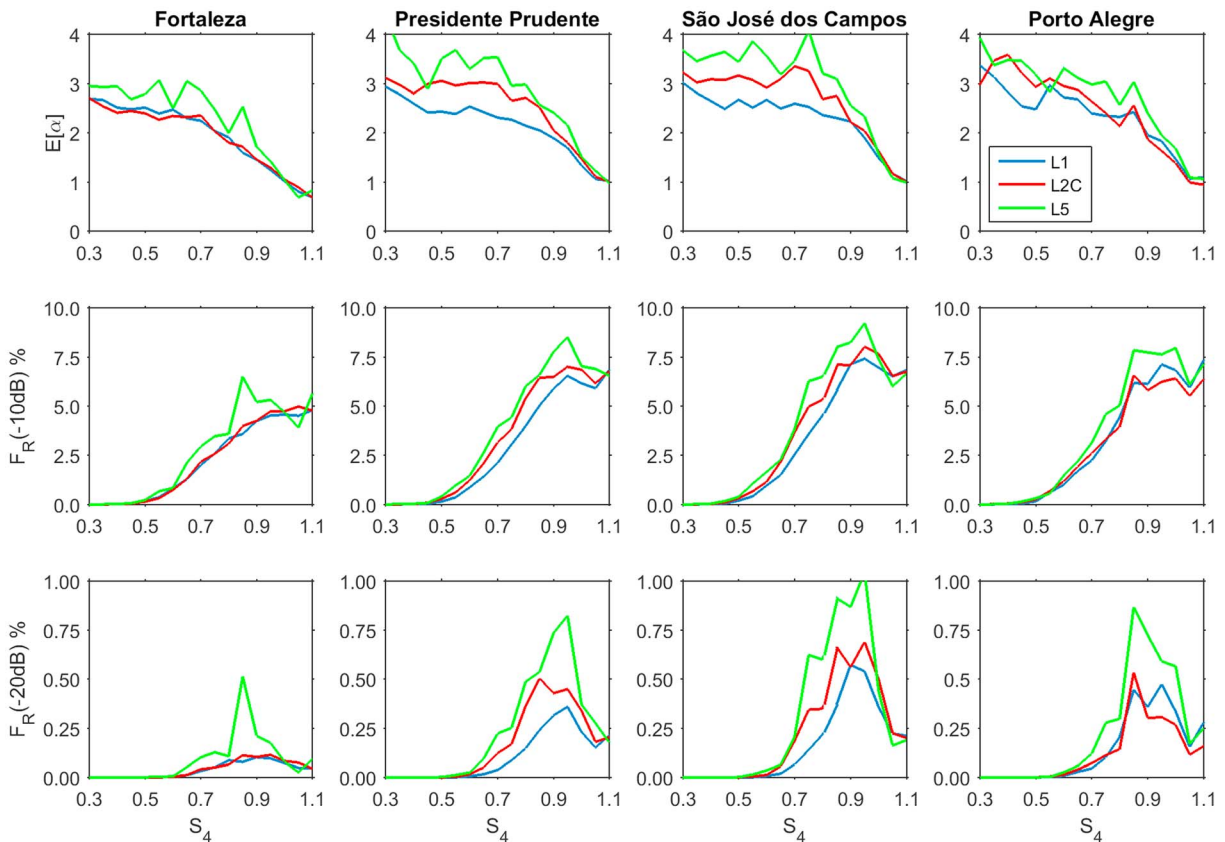


Figure 6. Upper row: Average values of α as functions of S_4 for different locations and GPS signals. Central and bottom rows: Curves of $F_R(r)$ (%) for -10 - and -20 -dB fades as functions of S_4 for different locations and GPS signals, respectively.

Table 4
Average Values and Standard Deviations of α in Different S_4 Intervals ($S_4 - 0.05, S_4 + 0.05$) and Locations for the L1, L2C, and L5 Signals

| S_4 | 0.3 | 0.4 | 0.5 | 0.6 | 0.7 | 0.8 | 0.9 | 1.0 | 1.1 |
|----------------------------|------|------|------|------|------|------|------|------|------|
| Fortaleza | | | | | | | | | |
| $E_{L1}[\alpha]$ | 2.68 | 2.51 | 2.51 | 2.47 | 2.24 | 1.91 | 1.45 | 1.01 | 0.68 |
| $E_{L2C}[\alpha]$ | 2.70 | 2.40 | 2.39 | 2.34 | 2.35 | 1.80 | 1.45 | 1.05 | 0.68 |
| $E_{L5}[\alpha]$ | 2.95 | 2.94 | 2.78 | 2.49 | 2.85 | 1.99 | 1.71 | 1.03 | 0.82 |
| $std_{L1}[\alpha]$ | 1.51 | 1.54 | 1.50 | 1.44 | 1.21 | 1.08 | 0.71 | 0.56 | 0.42 |
| $std_{L2C}[\alpha]$ | 1.49 | 1.40 | 1.31 | 1.27 | 1.19 | 0.80 | 0.62 | 0.43 | 0.32 |
| $std_{L5}[\alpha]$ | 1.63 | 1.85 | 1.62 | 1.49 | 1.45 | 1.23 | 0.86 | 0.60 | 0.47 |
| Presidente Prudente | | | | | | | | | |
| $E_{L1}[\alpha]$ | 2.65 | 2.31 | 2.04 | 2.18 | 2.04 | 1.86 | 1.74 | 1.28 | 1.03 |
| $E_{L2C}[\alpha]$ | 2.81 | 2.49 | 2.65 | 2.53 | 2.45 | 2.59 | 2.01 | 1.37 | 1.00 |
| $E_{L5}[\alpha]$ | 3.47 | 2.82 | 2.89 | 2.69 | 2.84 | 2.58 | 2.16 | 1.37 | 0.97 |
| $std_{L1}[\alpha]$ | 1.48 | 1.33 | 1.14 | 1.21 | 1.11 | 0.99 | 0.81 | 0.69 | 0.57 |
| $std_{L2C}[\alpha]$ | 1.59 | 1.58 | 1.47 | 1.41 | 1.37 | 1.07 | 0.82 | 0.69 | 0.57 |
| $std_{L5}[\alpha]$ | 1.99 | 1.62 | 1.73 | 1.60 | 1.67 | 1.07 | 0.83 | 0.75 | 0.59 |
| São José dos Campos | | | | | | | | | |
| $E_{L1}[\alpha]$ | 2.78 | 2.44 | 2.48 | 2.52 | 2.61 | 2.17 | 2.25 | 1.49 | 1.02 |
| $E_{L2C}[\alpha]$ | 3.01 | 2.74 | 2.90 | 2.75 | 2.83 | 2.39 | 2.01 | 1.50 | 0.99 |
| $E_{L5}[\alpha]$ | 3.05 | 2.87 | 2.66 | 3.32 | 2.76 | 2.73 | 2.25 | 1.47 | 1.02 |
| $std_{L1}[\alpha]$ | 1.63 | 1.60 | 1.42 | 1.40 | 1.28 | 1.19 | 0.92 | 0.80 | 0.61 |
| $std_{L2C}[\alpha]$ | 1.96 | 1.83 | 1.61 | 1.70 | 1.60 | 1.19 | 0.89 | 0.82 | 0.57 |
| $std_{L5}[\alpha]$ | 1.82 | 1.97 | 1.62 | 1.79 | 1.64 | 1.21 | 0.90 | 0.89 | 0.62 |
| Porto Alegre | | | | | | | | | |
| $E_{L1}[\alpha]$ | 3.23 | 2.88 | 2.39 | 2.74 | 2.41 | 2.32 | 1.71 | 1.35 | 1.08 |
| $E_{L2C}[\alpha]$ | 3.07 | 3.76 | 2.73 | 3.25 | 2.75 | 2.26 | 1.91 | 1.33 | 1.13 |
| $E_{L5}[\alpha]$ | 3.57 | 3.13 | 3.37 | 3.63 | 2.75 | 2.51 | 2.43 | 1.87 | 1.04 |
| $std_{L1}[\alpha]$ | 1.78 | 1.63 | 1.38 | 1.23 | 1.41 | 1.01 | 0.80 | 0.72 | 0.51 |
| $std_{L2C}[\alpha]$ | 1.99 | 2.43 | 1.52 | 1.87 | 1.91 | 1.19 | 0.82 | 0.53 | 0.53 |
| $std_{L5}[\alpha]$ | 2.30 | 2.47 | 1.68 | 2.18 | 1.35 | 1.10 | 0.75 | 0.77 | 0.63 |

$$F_R(r) = \frac{\Gamma(\mu, (r/\sqrt{\xi})^\alpha)}{\Gamma(\mu)}, \quad (4)$$

where $\Gamma(z, y) = \int_0^y t^{z-1} e^{-t} dt$ is the incomplete Gamma function. Equation (4) determines the probability of a fading event to be smaller than a threshold r . It is represented in the left plots of Figure 5 for two fixed values of S_4 (0.7 and 1.0) and different α values. The right plots show curves for $F_R(r)$ as a function of α , assuming two fixed values of S_4 (0.7 and 1.0) and different values of the signal intensity. Suppose a case where $S_4 = 0.95$ and $\alpha = 3.0$ ($\mu = 0.52$). According to equation (4) and the lower-left panel of Figure 5, the probability of a fading event deeper than 15 dB will be approximately equal to 4.7%. For the same S_4 value but $\alpha = 0.5$ ($\mu = 21.48$), the probability of a fading event deeper than 15 dB will decrease to 0.1%. This example indicates that the scintillation index S_4 alone does not describe the scenario for the satellite navigation user.

4. Fading Coefficients for the GPS L1, L2, and L5 Frequencies

The previous section presented the benefits of using the α - μ model for the statistical characterization of scintillation. In this section, the fading coefficients for the L1, L2C, and L5 signals and their association with the scintillation index S_4 will be described in more detail, with basis on the data from the four stations. Initially, Table 3 displays the percentages of S_4 occurrences in different intervals ($S_4 - 0.05, S_4 + 0.05$) and locations for the L1, L2C, and L5 signals. The central part of the first row of Table 3 indicates the centers of the S_4 intervals. The following rows indicate, for each location and GPS signal, the percentages of S_4 occurrence in the corresponding interval. The last two columns present, for each location and GPS signal, the percentages of noticeable ($S_4 \geq 0.3$) and moderate-to-strong

($S_4 \geq 0.5$) scintillation. It should be remembered that the percentages in Table 3 are calculated for the night hours 19h00 LT to 01h00 LT. Each line of Table 3 resulted from the processing of over 360.000 S_4 samples (1 min each), on average. The last two columns of Table 3 clearly shows that noticeable and moderate-to-strong scintillation more frequently affect the L2C and L5 signals than the L1 signal. They also show that scintillation occurs more frequently in signals received at PP than at SJ and FZ and less frequently at PA, depending on how close the stations are to the southern crest of the EIA.

It has been seen that the procedures described in the previous section provide associated S_4 , α , and μ estimates for each 1-min batch of the available data set. In continuation of the analysis of the above paragraph, the upper row of Figure 6 displays the average values of α as a function of S_4 for each location and GPS signal. To provide numbers that could be more easily applied to simulation models of scintillation effects on GPS signals, Table 4 displays the average values of α in the same S_4 intervals ($S_4 - 0.05, S_4 + 0.05$) and locations for the L1, L2C, and L5 signals. It is observed in Table 4 that the average α values for the L2C and L5 signals are greater than or equal to the corresponding ones for the L1 signal in 27 and 33 cases, respectively, out of the 36 available cases. Thus, the data confirm that the probability of deep fades increases as the frequency decreases, for any fixed value of S_4 . However, it is noted that, for all locations, the differences among the average α values for the three signals are relatively smaller for $S_4 \geq 0.9$ than those for $S_4 \leq 0.8$. Initially, the frequency was fixed and, for each value of S_4 , the greatest and smallest values of $E[\alpha]$ were determined from Table 4 or the upper row of Figure 6 among those associated with the four locations. The majority of the greatest values of $E[\alpha]$ so determined were associated with PA for all the signals, indicating that this location would experience the greatest occurrence of deep fades. On the other hand, the majority of the smallest values of $E[\alpha]$ were associated with PP for the L1 signal and FZ for the L2C and L5 signals, suggesting that these locations would be less affected by deep fading at these respective frequencies. Next, the location was fixed and, for each value of S_4 , the greatest and smallest values of $E[\alpha]$ were determined from Table 4

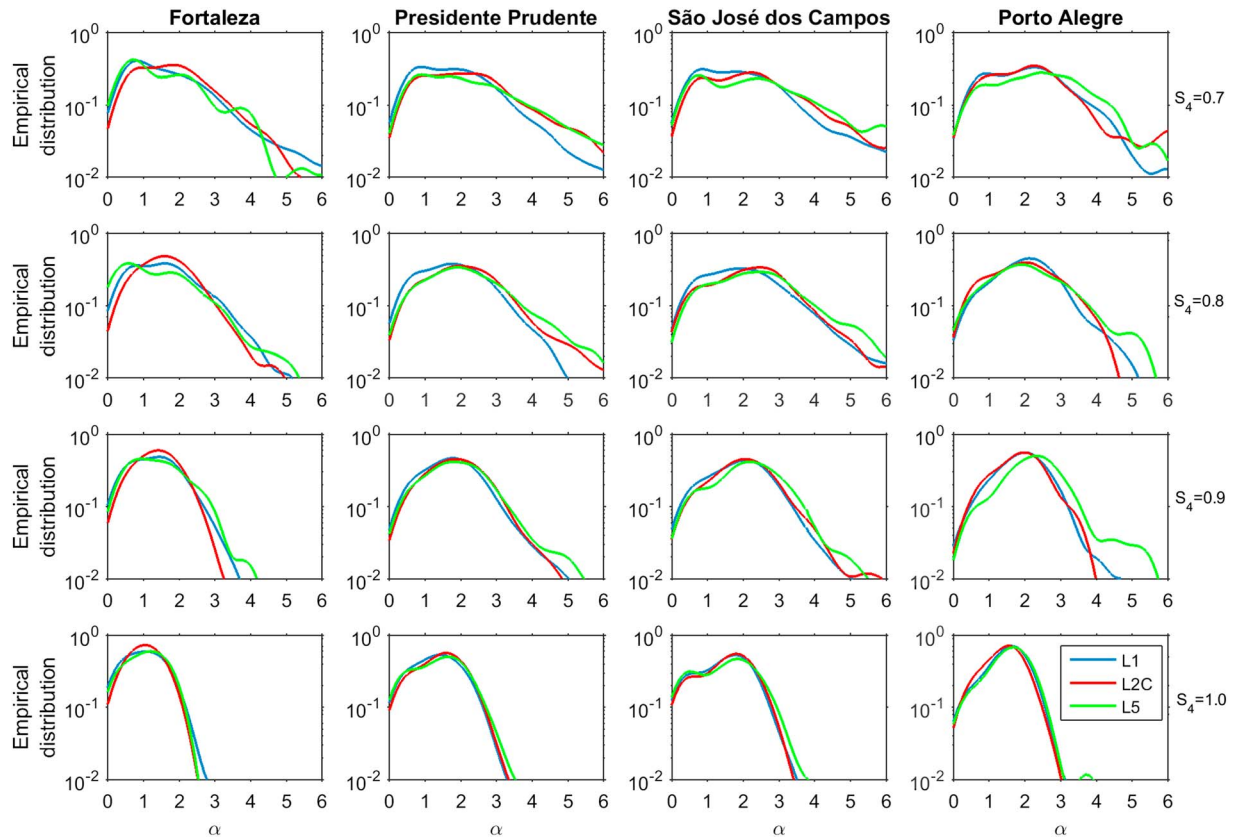


Figure 7. Empirical probability distribution functions of α for different values of S_4 intervals ($S_4 - 0.05$, $S_4 + 0.05$), locations, and GPS signals.

or the upper row of Figure 6 among those associated with the three frequencies. The majority of the greatest values of $E[\alpha]$ so determined were associated with the L5 signals for all locations, indicating that this frequency would experience the greatest occurrence of deep fades. However, the majority of the smallest values of $E[\alpha]$ were associated with the L2C signal for FZ and the L1 signal for the other three locations. These results, which can also be obtained by visual inspection of the upper row of Figure 6, confirm that the L5 and L2C signals are the most and least affected by deep fades, respectively. The central and bottom rows of Figure 6 show curves of the probabilities $F_R(-10 \text{ dB})$ and $F_R(-20 \text{ dB})$ of fades deeper than the corresponding arguments as functions of S_4 . To determine each point of these curves, equation (3) initially provides the value of μ associated with the pair $(S_4, E[\alpha])$, where $E[\alpha]$ is read from the Table 4 or the upper row of Figure 6 for the corresponding frequency and location. Equation (4) is then applied with the parameters $E[\alpha]$ and μ , as well as with the desired fade level. It is observed that the L5 signal has the greatest probability of experiencing fades deeper than -10 dB for $0.8 < S_4 < 1.0$, reaching 8.0% at PP and SJ, 7.5% at PA, and 6.5% at FZ. The corresponding probabilities are 1% to 2% less at the other frequencies. The bottom row of Figure 6 shows the probabilities of fades deeper than -20 dB . It is again observed that the critical region is in the interval $0.8 < S_4 < 1.0$. The probability of fades deeper than -20 dB in this S_4 interval reaches 0.9% and 0.8% at PP and SJ, for the L5 signal. The same probability is substantially less for the other signals, in particular at FZ.

Table 4 also shows the standard deviation of α , which measures the width of the corresponding parameter for each location and signal. Repeating the same processing of the previous paragraph, the frequency was initially fixed and, for each value of S_4 , the greatest and smallest values of $\text{std}[\alpha]$ were determined from Table 4 among those associated with the four locations. The majorities of the greatest and smallest values of $\text{std}[\alpha]$ so determined for the L1 signal were associated with SJ and PP, respectively. On the other hand, the majority of the greatest and smallest values of $\text{std}[\alpha]$ were associated with PA and FZ, for the L2C and L5 signals. Next, the location was fixed and, for each value of S_4 , the greatest and smallest values of $\text{std}[\alpha]$ were determined from

Table 4 among those associated with the three frequencies. The majority of the greatest values of $\text{std}[\alpha]$ were always associated with the L5 signals for all locations. However, the majority of the smallest values of $\text{std}[\alpha]$ were associated with the L2C signal for FZ and the L1 signal for the other three locations. The differences among the $\text{std}[\alpha]$ values for the three signals are also relatively smaller for $S_4 \geq 0.9$ than those for $S_4 \leq 0.8$.

Each panel of Figure 7 shows full pdfs of α value for each station and relatively high value of S_4 , for all signals. It is observed that the pdfs are not symmetrical around their maxima and that, for all locations and signals, dispersion of a set decreases as S_4 increases. The plots confirm the last observation of the previous paragraph. It is important to note that high values of α are more frequent for L2C and L5, in particular for PP and SJ, with $S_4 \leq 0.9$. This is an evidence that L2C and L5 signals will be more degraded and availability issues will be more frequent for users of those signals.

5. Conclusions and Final Remarks

In this work we analyzed the effects of ionospheric scintillation on the GPS signals received at L1, L2C, and L5 frequencies. Scintillation measurements were obtained with GPS receivers located in four stations distributed over the Brazilian sector (FZ, PP, SJ, and PA) at latitudes near and around the southern crest of the EIA. The Brazilian region where these stations are located has great dependence on satellite-based navigation systems, applied in activities such as precise agriculture, aviation traffic management, and oil rig operation. This study addressed important questions concerning the relatively more severe degradation effects suffered by the new L2C and L5 GPS signals, which have carriers with lower frequencies than that of traditional L1 signal, in respect of increasing scintillation index as well as deep fading effects caused by extreme scintillation events. The main conclusions of this study may be summarized as follows:

1. The analysis results showed that in the region near the equatorial anomaly crest, such as that monitored by the PP station, the chances of the L1 signal to be affected by moderate-to-strong scintillation events with $S_4 \geq 0.5$ are near 12%. For the L2C and L5 signals the value chances increase to above 17%. Thus, users of the new GPS signals L2C and L5 are more susceptible to be impacted by ionospheric irregularities.
2. The statistics of fading scintillation events verified how degraded the new signals at L2C and L5 can be in comparison to the L1 signal. By using the amplitude distribution model of α - μ distribution, a flexible fading model, it was found that the L5 signals (dedicated for safety-of-life applications) experienced highest probability of fades deeper than -10 dB, the probability for the range $0.8 \leq S_4 \leq 1.0$, reaching up to 8.0% at PP and SJ, and 7.5% and 6.5%, respectively, at PA and FZ. For the case of fades deeper than 20 dB this probability was around 1%. The L2 signal was less affected than L5 but generally more affected than L1 signal for which the probability was 1% to 2% less than that of L5.

Finally, analyzing the distribution of fading coefficients, it was observed that higher values of α are more frequent in L2C and especially at L5 signals than compared to L1. As higher α represents more severe fading, these signals are expected to face more problems in signal tracking and data demodulation.

Acknowledgments

This work is supported by Conselho Nacional de Desenvolvimento Científico e Tecnológico (CNPq) under award (INCT) 465648/2014-2 and FAPESP 2017/50115-0. E. Costa is supported by CNPq award (PQ) 309013/2016-0. J. Sousasantos acknowledges CAPES for the financial support. M. A. Abdu acknowledges the CAPES support for a senior visiting professorship at ITA/DCTA. F. Rodrigues would like to thank the support from NSF through award AST-1547048. The monitoring stations were deployed in the context of Projects CIGALA/CALIBRA, funded by the European Commission (EC) in the framework of FP7-GALILEO-2009-GSA and FP7-GALILEO-2011-GSA-1a, respectively, and FAPESP project 06/04008-2. The authors thank the reviewers for the insightful and constructive comments that helped them in the development of a better paper, as well as Michel Yacoub, Waldecir J. Perrella, Eurico de Paula and JHA Sobral for enlightening discussions on the α - μ distribution and geophysical aspects. The raw data used in this paper are available to be downloaded through the CIGALA/CALIRA website: <http://is-cigala-calibra.fct.unesp.br/is/index.php>.

References

- Abdu, M. A., Batista, I. S., & Sobral, J. H. A. (1992). A new aspect of magnetic declination control on equatorial spread-F and F region dynamo. *Journal of Geophysical Research*, 97(A10), 14,897–14,904. <https://doi.org/10.1029/92JA00826>
- Banerjee, P. K., Dabas, R. S., & Reddy, B. M. (1992). C and L band transionospheric scintillation experiment: Some results for applications to satellite radio systems. *Radio Science*, 27(6), 955–969. <https://doi.org/10.1029/92RS01307>
- Conker, R. S., El-Arini, M. B., Hegarty, C. J., & Hsiao, T. (2003). Modeling the effects of ionospheric scintillation on GPS/Satellite-Based Augmentation System availability. *Radio Science*, 38(1), 1001. <https://doi.org/10.1029/2000RS002604>
- Fremouw, E. J., Leadabrand, R. L., Livingston, R. C., Cousins, M. D., Rino, C. L., Fair, B. C., & Long, R. A. (1978). Early results from the DNA Wideband satellite experiment—Complex-signal scintillation. *Radio Science*, 13(1), 167–187. <https://doi.org/10.1029/RS013i001p00167>
- Hernández-Pajares, M., Juan, J. M., Sanz, J., Orus, R., García-Rigo, A., Felten, J., et al. (2009). The IGS VTEC maps: A reliable source of ionospheric information since. *Journal of Geodesy*, 83(3-4), 263–275. <https://doi.org/10.1007/s00190-008-0266-1>
- Humphreys, T. E., Psiaki, M. L., Hinks, J. C., O'Hanlon, B., & Kintner, P. M. Jr. (2009). Simulating ionosphere-induced scintillation for testing GPS receiver phase tracking loops. *IEEE Journal on Selected Topics in Signal Processing*, 3(4), 707–715. <https://doi.org/10.1109/JSTSP.2009.2024130>
- Jiao, Y., Xu, D., Morton, Y., & Rino, C. (2016). Equatorial scintillation amplitude fading characteristics across the GPS frequency bands. *Journal of the Institute of Navigation*, 63(3), 267–281. <https://doi.org/10.1002/navi.146>
- Moraes, A. O., Costa, E., Abdu, M. A., Rodrigues, F. S., de Paula, E. R., Oliveira, K., & Perrella, W. J. (2017). The variability of low-latitude ionospheric amplitude and phase scintillation detected by a triple-frequency GPS receiver. *Radio Science*, 52, 439–460. <https://doi.org/10.1002/2016RS006165>

- Moraes, A. O., Costa, E., de Paula, E. R., Perrella, W. J., & Monico, J. F. G. (2014). Extended ionospheric amplitude scintillation model for GPS receivers. *Radio Science*, *49*, 315–329. <https://doi.org/10.1002/2013RS005307>
- Moraes, A. O., de Paula, E. R., Muella, M. T. A. H., & Perrella, W. J. (2014). On the second order statistics for GPS ionospheric scintillation modeling. *Radio Science*, *49*, 94–105. <https://doi.org/10.1002/2013RS005270>
- Moraes, A. O., Muella, M. T. A. H., de Paula, E. R., de Oliveira, C. B. A., Terra, W. P., Perrella, W. J., & Meinbach-Rosa, P. R. P. (2017). Statistical evaluation of GLONASS amplitude scintillation over low latitudes in the Brazilian territory. *Advances in Space Research*, *61*(7), 1776–1789. <https://doi.org/10.1016/j.asr.2017.09.032>
- Moraes, A. O., de Paula, E. R., Perrella, W. J., & Rodrigues, F. S. (2012). On the distribution of GPS signal amplitudes during the low-latitude ionospheric scintillation. *GPS Solutions*, *17*(4), 499–510. <https://doi.org/10.1007/s10291-012-0295-3>
- Moraes, A. O., Vani, B. C., Costa, E., Abdu, M. A., de Paula, E. R., Sousasantos, J., et al. (2018). GPS availability and positioning issues when the signal paths are aligned with ionospheric plasma bubbles. *GPS Solutions*, *22*(4), 95. <https://doi.org/10.1007/s10291-018-0760-8>
- Seo, J., Walter, T., & Enge, P. (2011). Availability impact on GPS aviation due to strong ionospheric scintillation. *IEEE Transactions on Aerospace and Electronic Systems*, *47*(3), 1963–1973. <https://doi.org/10.1109/TAES.2011.5937276>
- Vani, B. C., Shimabukuro, M. H., & Monico, J. F. G. (2016). Visual exploration and analysis of ionospheric scintillation monitoring data: The ISMR query tool. *Computers and Geosciences*, *104*, 125–134. <https://doi.org/10.1016/j.cageo.2016.08.022>
- Venables, W. N., & Ripley, B. D. (2002). *Modern Applied Statistics with S* (4th ed.). New York: Springer.
- Yacoub, M. D. (2007). The α - μ distribution: A physical fading model for the Stacy distribution. *IEEE Transactions on Vehicular Technology*, *56*(1), 27–34. <https://doi.org/10.1109/TVT.2006.883753>
- Yeh, K. C., & Liu, C.-H. (1982). Radio wave scintillations in the ionosphere, *Proceedings of the IEEE*, *70*(4), 324–360. <https://doi.org/10.1109/PROC.1982.12313>, <https://ieeexplore.ieee.org/document/1456581/>